THE ASTRONOMICAL JOURNAL, 115:525–534, 1998 February

ROSAT OBSERVATIONS OF X-RAY–FAINT S0 GALAXIES: NGC 1380

ERIC M. SCHLEGEL,[1] ROBERT PETRE,[2] AND MICHAEL LOEWENSTEIN[2,3]

Received 1997 August 31; revised 1997 October 21

ABSTRACT

We used the *ROSAT* Position Sensitive Proportional Counter (PSPC) to obtain a 13 ks exposure and the *ROSAT* HRI to obtain a 42.5 ks exposure of the faint S0 galaxy NGC 1380. We show that the PSPC spectrum can be modeled as a thermal spectrum with $kT \sim 0.5$ keV, which is consistent with emission from a hot interstellar medium. We do not detect any emission from a hard component; the 90% upper limit is consistent with the trend for the scaled-up luminosities of X-ray–emitting point sources. The radial profiles from the PSPC and HRI data support the spectral fitting, because each profile is more sharply concentrated than the optical light (which reflects the stellar distribution), in contrast to other E/S0 galaxies. The PSPC radial profile is consistent with emission from a point source, because of the larger point-spread function; the HRI profile reveals the presence of extended hot gas. We also extend the L_X-L_B plane, described by Matsumoto et al. in the range $10.8 < \log L_B < 11.3$, to $\log L_B \sim 10.5$. We extend this plane separately for the hard discrete and the soft thermal components and show that the scaling relation for the hard component continues to at least $\log L_B \sim 10.5$.

Key words: galaxies: individual (NGC 1380) — X-rays

1. INTRODUCTION

S0 and E galaxies were first detected as X-ray sources by the *Einstein* satellite (for a review, see Fabbiano 1989 and references therein). A relationship exists (Fig. 1) between the X-ray luminosity and the blue optical luminosity of these galaxies, such that

$$\frac{L_X}{10^{41}\ \mathrm{ergs\ s^{-1}}} \sim 0.94\left(\frac{L_B}{10^{11}\ L_\odot}\right)^{2.27} \quad (1)$$

(see Sarazin 1990 or Eskridge, Fabbiano, & Kim 1995, and references therein), for L_X defined in the 0.5–4.5 keV band, where the distances of Donnelly, Faber, & O'Connell (1990) have been used, and where the blue-band luminosity, in solar units, is defined by $\log L_B = -0.4(M_B - 5.41)$, as in Matsumoto et al. (1997). There is a suggestion of an upward break in Figure 1 at $L_B \sim 10^{10.8}$. White & Davis (1997) did not see this break in their analysis of a nearly complete (98%) sample of elliptical galaxies observed with the *ROSAT* Position Sensitive Proportional Counter (PSPC; Davis & White 1997), because their sample only extended to $L_B \sim 10^{11}$. If we take Figure 1 at face value, however, we expect distinctly different spectral properties between the most and the least luminous galaxies. To date, with one exception, all presentations of the L_X-L_B diagram have used a total $L_X = L_X^{\mathrm{hard}} + L_X^{\mathrm{soft}}$. Matsumoto et al. (1997) first presented the L_X-L_B plane separately for L_X^{hard} and L_X^{soft}. A goal of this paper is the extension of this plane to lower luminosities.

The most luminous galaxies, with $L_X \sim 10^{41}$–10^{42} ergs $\mathrm{s^{-1}}$, have thermal spectra that peak at $kT \sim 1$ keV (see, e.g., Kim et al. 1992). This thermal component, hereafter described as the "soft" component, is emission from a hot, optically thin gas. Intrinsic dispersion, of at least an order of magnitude, exists in the L_X values of the soft component for $L_B > 3 \times 10^{10}\ L_\odot$ (see, e.g., Matsumoto et al. 1997; Donnelly et al. 1990). Models to explain the dispersion are described in, for example, White & Sarazin (1991) and Ciotti et al. (1991).

A hard component is also expected to contribute to the total L_X. The contribution of X-ray–emitting point sources, if scaled up to the luminosities of equation (1) from observations of Galactic sources, is

$$\frac{L_X}{10^{41}\ \mathrm{ergs\ s^{-1}}} \sim K\ \frac{L_B}{10^{11}\ L_\odot}, \quad (2)$$

with $K = 0.42$ (Fabbiano, Gioia, & Trinchieri 1989), 0.33 (Canizares, Fabbiano, & Trinchieri 1987), or 0.04 (Forman, Jones, & Tucker 1985). Matsumoto et al. (1997) have recently shown that K is $\sim$0.3–0.4 for $\log L_B > 10.8$, by spectrally separating the hard component using broadband spectra from *ASCA*.

Kim et al. (1992) anticipated the results of the spectral separation by dividing the E/S0 galaxies into four luminosity bins based on the value of the ratio of the X-ray luminosity to the blue optical luminosity, L_X/L_B (highest ratio = group 4, lowest ratio = group 1). The galaxies in groups 3 and 4 show X-ray spectra that peak at $\sim$1 keV, indicative of a hot, optically thin interstellar medium (ISM; Fabbiano 1994). The group 1 and 2 galaxies have spectra that resemble spiral galaxies, i.e., relatively hard spectra typical of X-ray binaries. Fabbiano, Kim, & Trinchieri (1994) presented evidence for the existence of a very soft ($kT \sim 0.2$ keV) component in the *ROSAT* PSPC spectra of the group 1 galaxies NGC 4365 and NGC 4382. This evidence was confirmed by Kim et al. (1996) in their analysis of the *ASCA* spectrum of NGC 4382. The nature of this very soft component is not clear (Pellegrini & Fabbiano 1994).

In this paper, we report on the X-ray emission from the S0 galaxy NGC 1380, as detected by the *ROSAT* PSPC. NGC 1380 was not included in the survey of Davis & White (1996, 1997). The first *ROSAT* image of NGC 1380 was presented in Schlegel & Petre (1993), which reported on an upper limit to the X-ray emission of supernova SN 1992A. NGC 1380 has $\log L_X \sim 40.55$ and $\log L_B \sim 10.59$, placing it, within the scatter, near the break point of the L_X-L_B

[1] Smithsonian Astrophysical Observatory, Mail Stop 4, 60 Garden Street, Cambridge, MA 02138.
[2] NASA Goddard Space Flight Center, Code 662, Greenbelt, MD 20771.
[3] Also Research Scientist, University of Maryland.

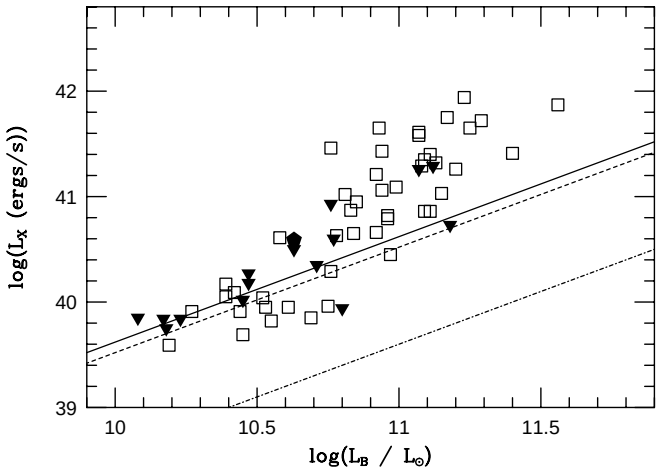

FIG. 1.—L_X/L_B plot, with NGC 1380 indicated by a pentagon. Triangles represent upper limits. Lines represent the scaled-up stellar luminosities (eq. [2]) with $K = 0.42$, 0.33, 0.04 (*top to bottom*). Data from Donnelly et al. (1990).

relation of Figure 1, but still in group 1. The distance to the galaxy is assumed to be 27.5 Mpc (Donnelly et al. 1990), with $H_0 = 50\ \mathrm{km\ s^{-1}\ Mpc^{-1}}$.

Section 2 describes the PSPC and HRI observations of NGC 1380, while § 3 contains the analysis of the PSPC spectrum. Section 4 discusses the results of the NGC 1380 observation in the context of other S0 and E galaxies observed with *ASCA*.

2. DESCRIPTION OF THE OBSERVATIONS

2.1. *PSPC Data*

NGC 1380 was observed with the PSPC (Pfeffermann et al. 1987) on *ROSAT* (sequence RP600127) with an on-axis pointing at NGC 1380 for an exposure of 17,355 s. The housekeeping data showed that a different roll angle was used for the last few observation intervals (OBIs); these OBIs were filtered out of the data. The filtering also removed a possible short-term enhancement (Snowden et al. 1994), as the last OBIs had an $\sim 80\%$ higher count rate than the other OBIs. Within the counting errors, the count rates of the remaining OBIs were constant to within 10% averaged over the entire field. After these OBIs were filtered from the data set, the net exposure time was 13,658 s. The spectrum of the background showed no sign of an afterpulse (Snowden et al. 1994) nor any evidence of additional short- or long-term fluctuations.

Since NGC 1380 was observed on-axis, vignetting corrections are negligible, particularly for a source with such a small angular size ($\sim 2'$). Figure 2 shows the PSPC contours overlaid on an optical image[4] of NGC 1380. The contours are centered on the nucleus of the galaxy. There is a suggestion of extended emission in the outermost contours, but the overall radial profile is basically consistent with the point-spread function (PSF) of the PSPC (Hasinger et al. 1994). The 50% radius for the X-ray emission is $\sim 20''$, which is consistent within the errors with a pointlike source. As the optical 50% radius along the minor axis is $\sim 60''$, we conclude that the optical and X-ray emission are not distributed identically. Although we do not present the image, we note that there are no detected counts above ~ 1.8 keV at the location of NGC 1380 that can be attributed to NGC 1380 itself. In other words, above ~ 1.8 keV, all of the X-ray photons are consistent with the X-ray background or the extended, hard emission from the center of the Fornax Cluster. That comment stands in contrast to a conclusion by Jones et al. (1997) in their analysis of the Fornax Cluster emission. They state that NGC 1380 is the only one of 13 Fornax galaxies that has a hard spectrum. The Jones et al. observation was centered on NGC 1399; NGC 1380 lies $\sim 40'$ away. We believe the source of the discrepancy lies in the large off-axis angle: vignetting will preferentially remove hard photons from the off-axis source, and the particular value of the off-axis angle places NGC 1380 near or under the main support ring and rib structure. This structure will block harder photons. Jones et al. correct for vignetting and the reduced exposure; however, their correction is very likely an overcorrection, leading them to conclude that NGC 1380 has a hard spectrum.

[4] The optical image was obtained using the SkyView facility of HEASARC, NASA Goddard Space Flight Center.

2.2. *HRI Observations*

The HRI was used to observe NGC 1380 on 1995 July 25–27 for 42 ks. The data were processed with the diffuse emission code of Snowden (1995). The dead-time–corrected, processed data had an exposure time of 42,526 s. A total of 358 counts were collected at the position of NGC 1380. The data were then smoothed with a Gaussian distribution with FWHM of $2''$. Figure 3 shows the contours of the smoothed HRI data overlaid on the SkyView optical image of NGC 1380. The X-ray emission arises from a region near the projected center of the galaxy. Figure 4*a* shows cuts made along the major and minor axes, using bins of width $2''$ that extended a total of $\sim 30''$ outward from the nucleus. Overall, the two profile cuts are similar in appearance. The cuts quantify the asymmetries of the X-ray emission toward the south and toward the east.

Figure 4*b* (*top*) shows the azimuthally integrated profile obtained by extracting the counts in annuli $2''$ wide. The emission is centered on the nucleus but is more extended than the PSF (*solid line*; David et al. 1996). We note that a weak point source located $\sim 6'$ off-axis is consistent with the PSF at that location, so there are no systematic aspect errors. We do note that if the theoretical PSF is raised to the top of the error bar range for the innermost point, there is evidence for a point source at the center. The possible point source would still be surrounded by extended emission. As we shall show, this possible point source must itself be a soft source.

Regardless, the profile disappears into the background about $20''$ from the center. The "plateau" at about $15''$ arises from the broad shelf in the contours that extends east of the nuclear region (Fig. 3). For a comparison, we include the profile from the PSPC data in Figure 4*b* (*bottom*). The small size of the X-ray–emitting region as detected by the HRI is supported by the pointlike appearance in the PSPC data. The difference between the X-ray and optical radial profiles of NGC 1380 stands in contrast to the corresponding profiles of other E/S0 galaxies. Fabbiano, Trinchieri, & Canizares (1986) compared *Einstein* IPC profiles with optical profiles for four E/S0 galaxies. The profiles behaved identically out to between $5'$ and $8'$. Trinchieri et al. (1994) found the same behavior for NGC 4636 in a comparison of *ROSAT* PSPC observations with optical data. Note that no

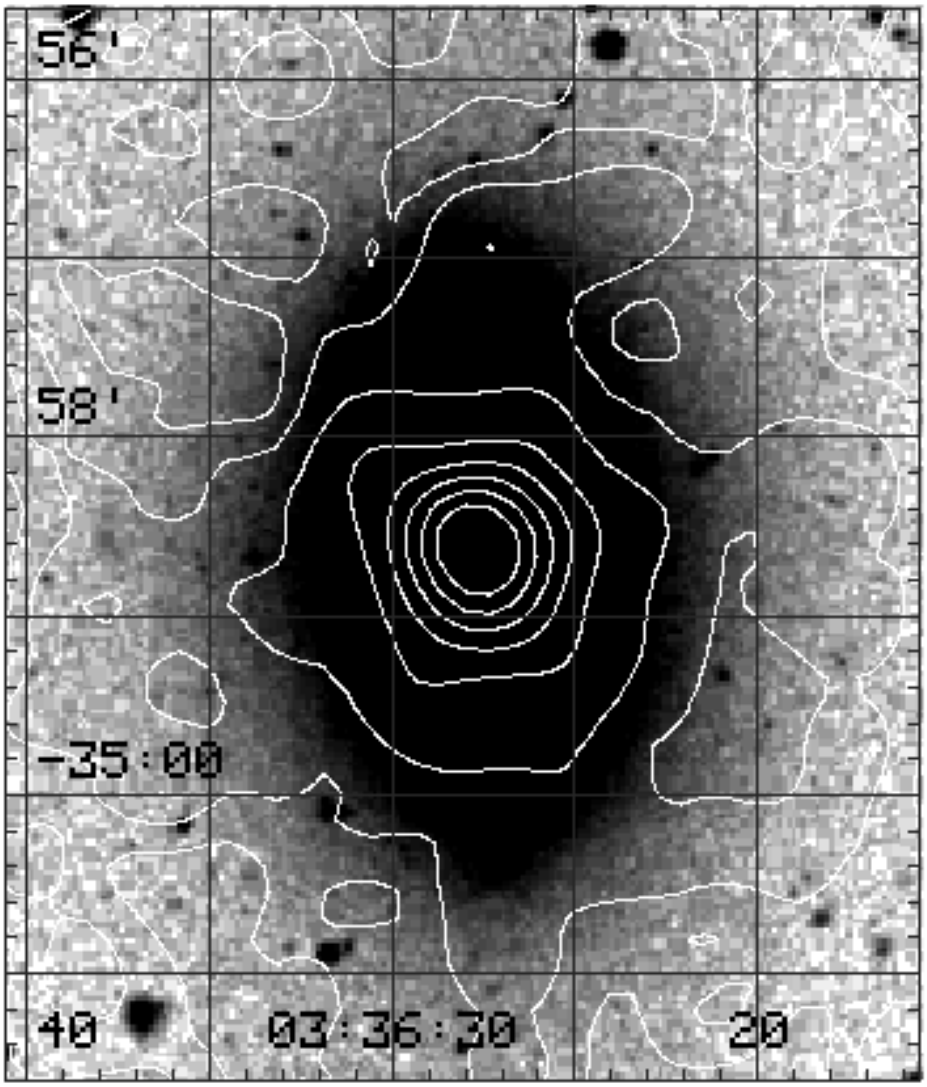

FIG. 2.—PSPC image (*contours*) overlaid on an optical image of NGC 1380. The contours define the following levels starting at the image center: 6.0, 5.0, 4.0, 3.0, 2.0, 1.0, 0.5, and 0.3 counts arcmin^{-2}. The background level is $\sim$0.4 counts arcmin^{-2}. North is up and east is to the left. The image is $\sim$5′ on a side. The numbers along the bottom represent the right ascension; the numbers on the upper $\frac{3}{4}$ of the left side represent the declination.

systematic study has yet been made using *ROSAT* data. For NGC 1380 then, that the X-ray emission is not as extended as the optical light may indicate that NGC 1380 has lost (or is losing) X-ray–emitting material. The present data are insufficient to establish this possibility with certainty. We point out that the HRI would not detect an extended, hard, low surface brightness emission, because of its higher instrumental background.

The reader may consider it possible that the plateau to the east of the nucleus arises from the merger of the contours of a weak point source with the low-lying contours of the nuclear emission. The HRI PSF is sufficiently sharp, however, that a 3 σ point source would be separated from the distributed emission. The same comment applies to the southern asymmetry.

We do not apply the intrinsic isophotal shape analysis of, for example, Buote & Canizares (1996). The key assumption in shape analysis is that the isophotes are indicative of the gravitational potential undisturbed by neighbors. NGC 1380 is a member of the Fornax Cluster and is sufficiently close to the cluster center that the assumption is invalidated.

3. SPECTRAL ANALYSIS

The fitting package XSPEC (version 9) was used for all of the analyses. Simple continuum models were folded through the detector response and compared with the data. We extracted the spectrum using a circular aperture of radius 1′ centered on the position of NGC 1380. This size was chosen after examining the azimuthally averaged profile of Figure 4*b*. A total of 530 ± 33 counts were extracted, yielding a count rate of 0.039 ± 0.002 counts s^{-1} for the 0.2–2.0 keV band of *ROSAT*. The number of counts is sufficiently low that no attempt to extract radially resolved spectra can be made; only the spectrum from the entire galaxy will be considered. The resulting spectrum was fitted using the basic models (Raymond, bremsstrahlung, power-law). We also attempted a two-component model, such as those advocated by Fabbiano et al. (1994).

We used two approaches to subtract the background, as a check that X-ray emission from the Fornax Cluster did not contaminate the spectrum. Using the first method, we subtracted the counts obtained from an annulus surrounding the galaxy from the raw source counts, leaving a net

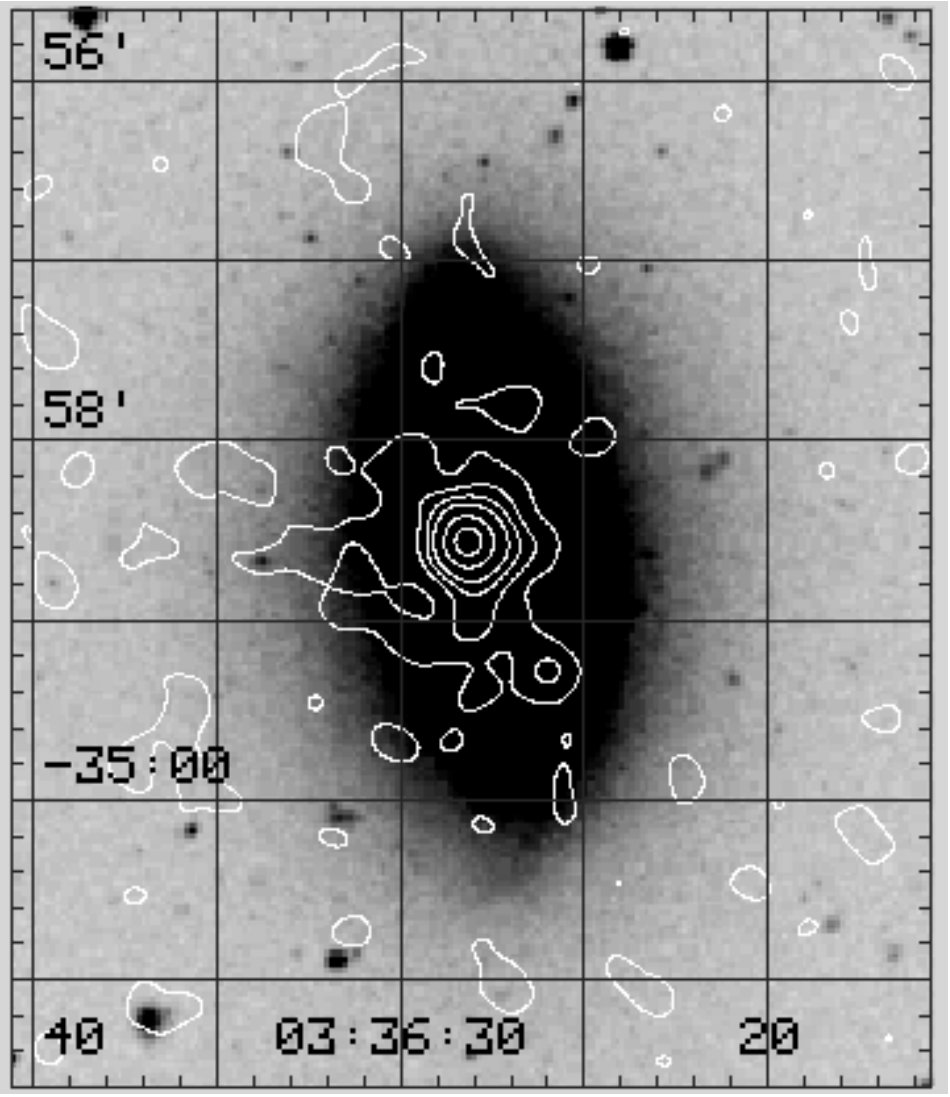

FIG. 3.—HRI image (*contours*) of NGC 1380 overlaid on an optical image of the galaxy. North is up and east is to the left. The image is $\sim 5'$ on a side. The contours define the following levels: 2.0, 1.5, 1.0, 0.75, 0.55, and 0.35 counts arcmin^{-2}.

source spectrum. In the second approach, we fitted the raw source and background spectra simultaneously. For the background model, we adopted the best-fit cosmic background model from the BBXRT data (Jahoda et al. 1992) and included a thermal bremsstrahlung component, fixed at the temperature (~ 1.2 keV) characteristic of the outer portions of the emission of the Fornax Cluster (Ikebe et al. 1996). The two background subtraction methods were in good agreement; the fitted values did not differ by more than 10%.

The power-law and Raymond models (with abundance fixed at solar) do not provide good fits to the data ($\chi^2/\nu = 1.26$ and 1.67, respectively). The thermal bremsstrahlung model provides a better fit ($\chi^2/\nu = 1.14$). Figure 5*a* shows the fitted bremsstrahlung model. The differences between the various models were slight, although the power-law model left clearly visible residuals near 0.9 keV. The 0.2–2.0 keV flux is 3.2×10^{-13} ergs s^{-1} cm^{-2}. At the adopted distance, this flux corresponds to a luminosity of $\sim 2.9 \times 10^{40}$ ergs s^{-1}. Figure 5*b* shows the contours of (kT, $N_{\rm H}$) for the bremsstrahlung model. The bremsstrahlung temperature yields a value for $\beta \equiv \mu m_{\rm H} \sigma^2/kT \sim 0.66$, with μ the mean molecular weight, with an adopted value of ~ 0.6, and σ the velocity dispersion, 225 km s^{-1} (Roberts et al. 1991). A β of 0.66 is not unusual (see, e.g., Matsumoto et al. 1997) for an early-type galaxy with similar values of $L_{\rm X}$ and σ. We now turn to some remarks on more complex models.

First, we return briefly to the Raymond model. If the overall metal abundance is permitted to vary, the Raymond model provides the best fit, with a χ^2/ν of 0.99. The fitted value of the abundance is ~ 0.026 (Table 1). For both the bremsstrahlung and the total abundance–varying Raymond models, the fitted temperatures and columns are nearly identical, with $kT \sim 0.5$ keV and $N_{\rm H} \sim 2 \times 10^{20}$ cm^{-2}. The fitted value for the column density is, within the errors, consistent with the known Galactic column (Stark et al. 1992). The fitted value of the abundance, for the best-fit temperature, matches the values and trend (abundance $\propto T^{2.4}$) found by White & Davis (1997) for other elliptical

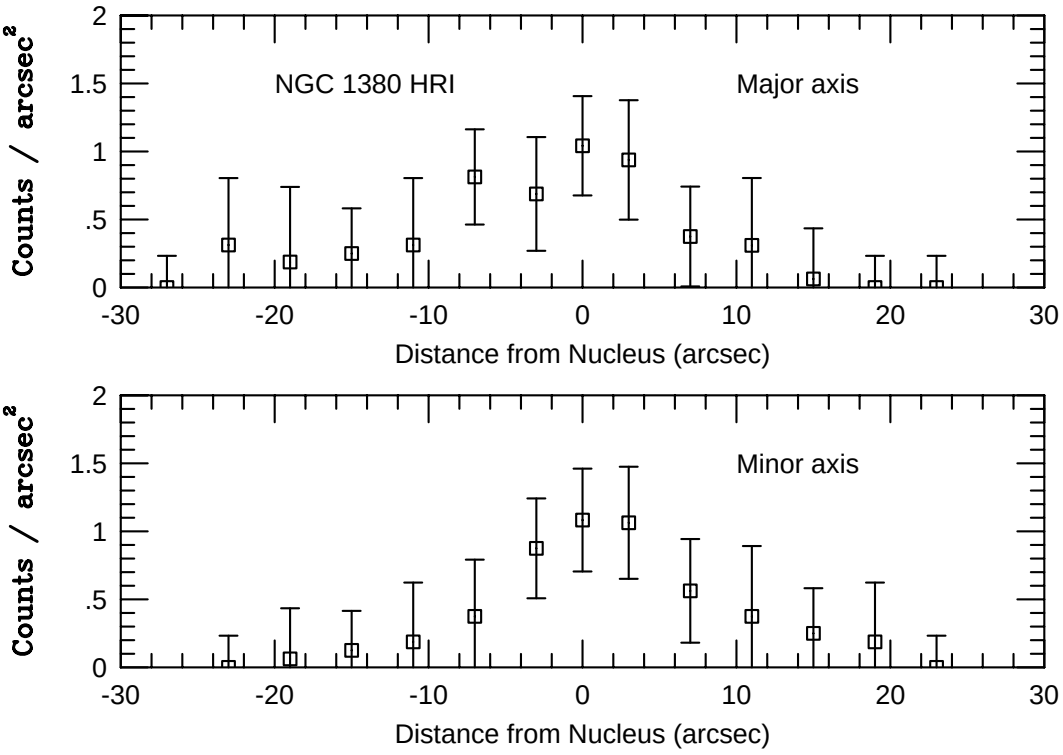

FIG. 4*a*

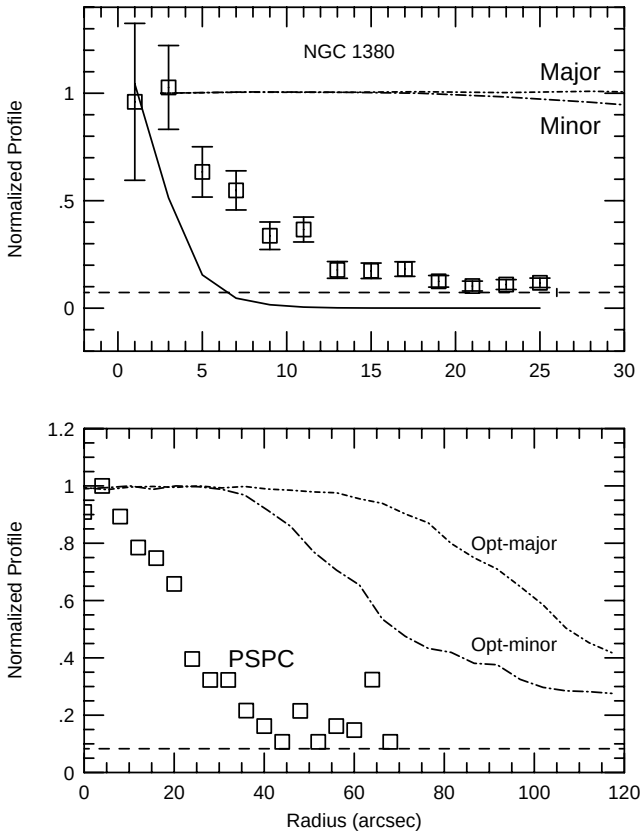

FIG. 4*b*

FIG. 4.—(*a*) Major- and minor-axis profiles of NGC 1380 as observed with the HRI. Negative distances from the nucleus lie to the south (major axis) or to the east (minor axis). (*b*) *Top*: Radial profile of NGC 1380 from the HRI data. The solid line illustrates the PSF (David et al. 1996). The dot-dashed lines labeled "Major" and "Minor" represent normalized profiles of the optical image of NGC 1380. As is visible in Figs. 2 and 3, the optical emission extends well beyond the X-ray emission as detected by the HRI. *Bottom*: Radial profile from the PSPC data (*squares*). The dashed line represents the background emission in a region near NGC 1380. The optical profiles are included for comparison.

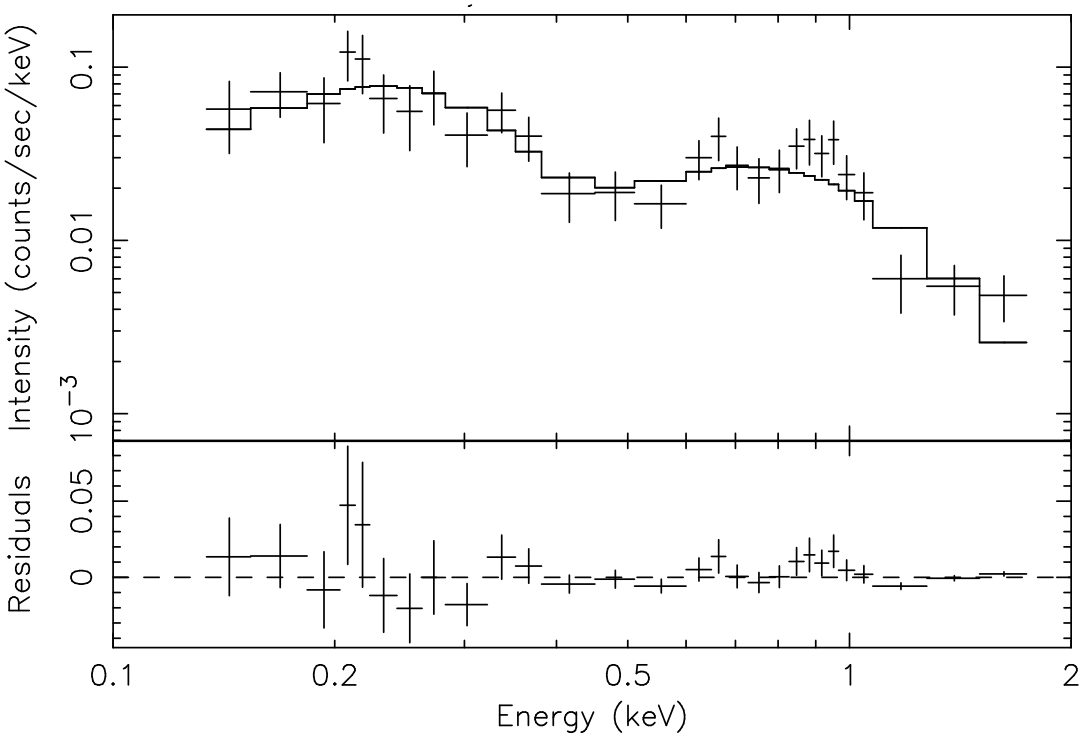

FIG. 5*a*

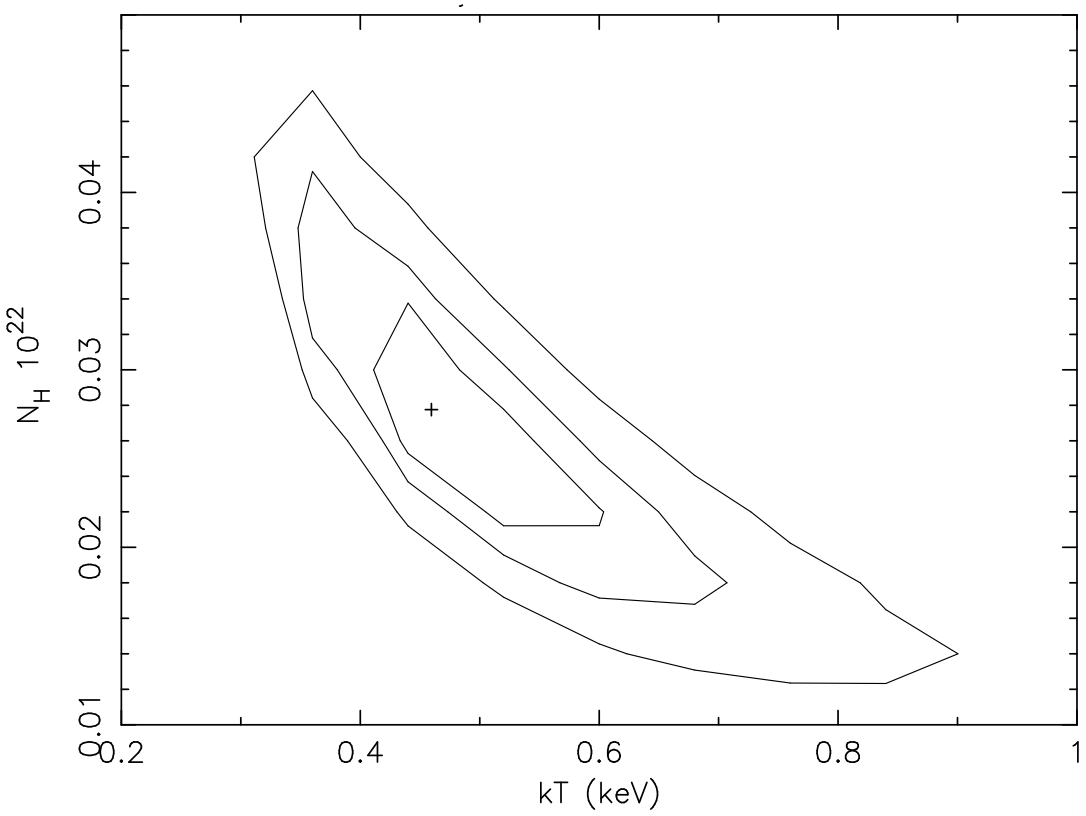

FIG. 5*b*

FIG. 5.—(*a*) Thermal bremsstrahlung model fitted to the PSPC spectrum of NGC 1380. The variable-abundance Raymond model looks nearly identical, except that the residuals in the 0.9 keV region are flatter. (*b*) Contour plot for the bremsstrahlung model. The contours are $\Delta\chi^2 = +2.30$, $+4.61$, and $+9.21$, corresponding to the 1 σ, 90%, and 99% levels for two parameters of interest.

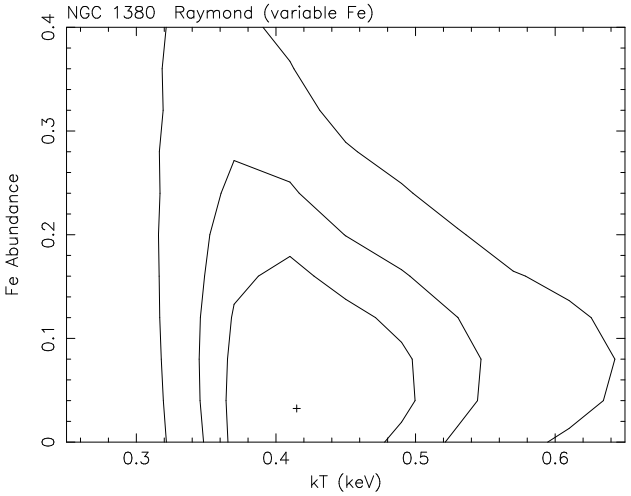

FIG. 6.—Contours of kT and Fe abundance of NGC 1380, for a model in which each element's abundance was permitted to vary (see text for details).

galaxies (their Fig. 4).[5] The T abundance correlation could indicate that more luminous galaxies have a higher supernova rate. It is known that, for Sbc–Sc galaxies,[6] the supernova rate is proportional to the parent galaxy luminosity (see van den Bergh & Tammann 1991 and references therein). Matsumoto et al. (1997) also conclude that the larger systems are more efficient at retaining hot gas and less efficient at converting it into stars.

Second, we also used a variable-abundance Raymond model in which the abundance of each element can be varied individually. There are insufficient counts to permit a global fit to all of the abundances, so we instead fixed all but one of the abundance values. We then fitted the model to the data and proceeded through the list of elements, varying each in turn to see if any were tightly constrained by the data. Only the abundance of Fe was constrained significantly to be less than 0.3 (95% confidence). Figure 6 shows the Fe abundance and temperature contours. The variation in the total abundance fit is dominated by the variation in the Fe abundance. The abundances of all of the other elements were consistent with unity. We do not suggest that Fe is the only element with a different abundance; the number of detected counts limits us to stating that the different abundance for Fe was the only one we could detect. The lower Fe abundance is consistent with the behavior detected from *ASCA* data for the bright elliptical galaxies, such as NGC 4374 or NGC 1404 (Matsushita et al. 1994; Loewenstein et al. 1994).

Finally, we tried the two-component model. We note that the extra degree of freedom of a variable-abundance model, regardless of whether it is a total or an element-specific variable abundance, can generally be matched in the quality of the fit by fitting the data with a two-component model. We tried a two-temperature fit; in all cases, however, the model either did not converge or the two temperatures converged on the same value. We conclude that for this NGC 1380 data set, the two-temperature model does not describe the spectrum.

A hard component is expected that represents the collective contribution of X-ray binaries. To test for the presence

[5] They did not find a corresponding correlation between their abundances and the stellar metallicity index (Mg_2), but that is not surprising, because the apertures used for the Mg_2 data are about an order of magnitude smaller than the "apertures" over which the X-ray counts were integrated. The two measures are therefore sensitive to different spatial scales.

[6] There are insufficient numbers of supernovae for a study across all types of galaxies.

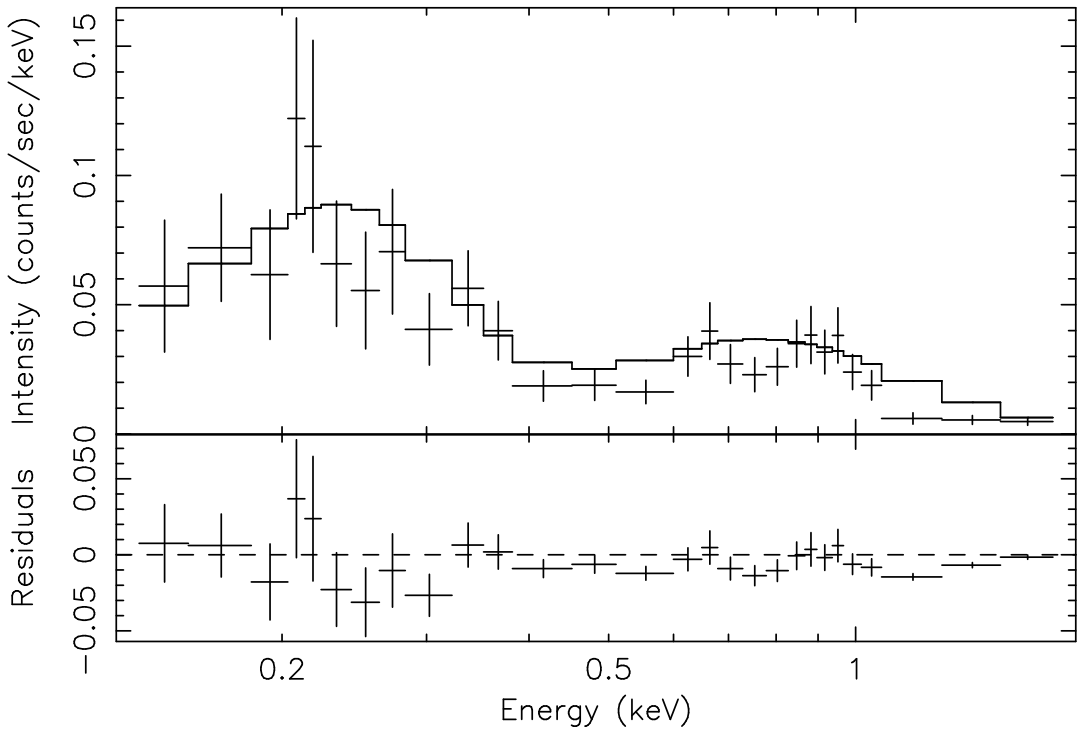

FIG. 7.—Fitted spectrum of Fig. 5 for NGC 1380, with an added component to represent the X-ray emission of X-ray binaries. The adopted temperature of the binary component is 5 keV. The spectrum illustrates the deviation of the model from the data for a 90% upper limit on the flux of the 5 keV component. Note the residuals above 1 keV, at $\sim$0.75 keV, and in the 0.5 keV region.

TABLE 1

FITTED MODELS FOR NGC 1380

Model	χ^2, ν	N_H (10^{20} cm^{-2})	α or kT	0.2–2.0 keV Flux (10^{-13} ergs s^{-1} cm^{-2})	Luminosity (10^{40} ergs s^{-1})
Power law	1.26, 25	$5.1^{+1.7}_{-1.6}$	$3.29^{+0.54}_{-0.44}$	...	...
Bremsstrahlung.....	1.14, 25	$2.8^{+0.6}_{-0.7}$	$0.46^{+0.13}_{-0.05}$	3.3	3
Raymond:					
Fixed[a].....	1.67, 25	$0^{+0.35}_{-0.0}$	$0.31^{+0.03}_{-0.04}$	...	...
Varying[b]	0.99, 24	$1.8^{+1.1}_{-0.9}$	$0.47^{+0.14}_{-0.10}$	2.9	2.6
Variable Fe[c]	0.99, 24	$0.15^{+0.30}_{-0.15}$	$0.41^{+0.09}_{-0.05}$	...	...

[a] The value for the abundance was fixed at 1.0.
[b] The value of the abundance was allowed to vary. The fitted value was $0.026^{+0.031}_{-0.013}$.
[c] Only the abundance of Fe was allowed to vary. The fitted value for the abundance was $0.033^{+0.150}_{-0.033}$.

of a hard tail in the spectrum, a bremsstrahlung component with $kT = 5$ keV was added to the best-fit model. The component's normalization was raised until $\Delta\chi^2$ increased by 2.71, the 90% confidence level for one parameter of interest. The 0.2–2.0 keV flux in that component was then calculated: its value is 1.4×10^{-13} ergs s^{-1} cm^{-2}, or a 0.2–2.0 keV luminosity of 1.3×10^{40} ergs s^{-1}. This flux is the 90% confidence upper limit to the existence of a hard tail resulting from the X-ray emission of X-ray binaries, for example. The luminosity is $\sim$40% of the 0.2–2.0 keV luminosity of the thermal component. Figure 7 illustrates the appearance of the spectrum with the additional component. The "residuals" caused by the introduction of the hard component are readily apparent. The lack of a hard component in the spectrum was already anticipated by the lack of any counts in the image when the image is filtered for counts $\gtrsim$1.8 keV.

4. DISCUSSION

The nature of the X-ray emission from E/S0 galaxies has been confirmed and dissected with *ROSAT* and *ASCA* data by many researchers (recent papers include Matsumoto et al. 1997; Davis & White 1997; White & Davis 1996; Kim et al. 1996; Matsushita et al. 1994; Pellegrini 1994; Pellegrini & Fabbiano 1994; Fabbiano et al. 1994). The HRI data presented here for NGC 1380 show that the emission is centered on the nucleus and is distributed smoothly, but not uniformly, about it. The PSPC data show that the spectrum is soft ($kT \sim 0.5$ keV) and the ISM gas is metal-poor (at least, the iron abundance is low). No evidence exists for a hard component in NGC 1380, although the upper limit from the PSPC data is consistent with the expected variation of $\sim$3 about the scaled luminosity of discrete sources (Canizares et al. 1987), and the high instrumental background of the HRI prevents us from assigning a more stringent value to the upper limit.

The primary diagnostic of the X-ray emission from E/S0 galaxies is the L_X-L_B plane (see Fig. 1). The upper end (log $L_B > 10.8$) of this diagram is well defined and has been presented in Matsumoto et al. (1997). Our primary interest is the extension of the observed L_X-L_B plane to luminosities log $L_B < 10.8$. We are interested to see if the luminosity of the hard component follows the scaling relations presented in § 1. We use the Matsumoto et al. (1997) sample from *ASCA* data, rather than more extensive samples in the literature, because the larger energy range of *ASCA* permits the separation of the soft and the hard emission components, which has not previously been possible.

In Figure 8, we present a subset of this diagram in which we plot the luminosities of the soft and hard components separately based upon fluxes from fitted models (Table 2).[7] We use the results presented in Matsumoto et al. (1997) here. The Matsumoto et al. galaxies have all been observed with *ASCA*; Matsumoto et al. extracted the data (12 galaxies) from the *ASCA* archive and remeasured the spectral parameters of the galaxies using an identical spectral model for all of them. To these data, we add three faint galaxies observed by *ASCA* from Loewenstein et al. (1997), and the *ROSAT* PSPC data on NGC 1380, the spectrum of which we corrected to the *ASCA* energy band (to be described shortly). The proper approach to the production of Figure 8 is the joint fitting of *ROSAT* PSPC and *ASCA* spectra to measure accurately the spectral shapes of the hard and soft components. A more accurate description of

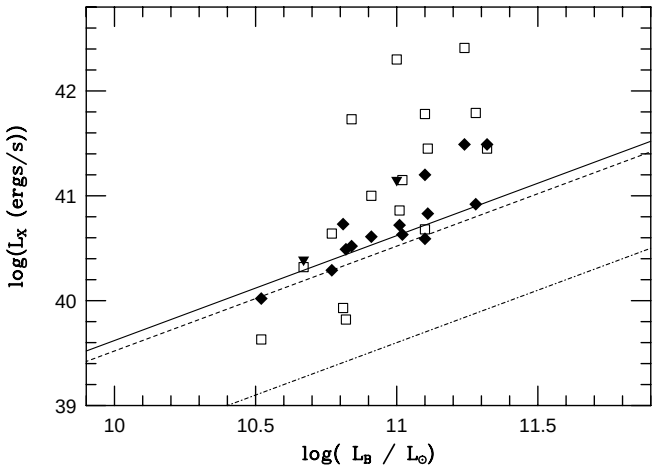

FIG. 8.—L_X-L_B plane separated into hard (*diamonds*) and soft (*squares*) components. We have used the distances from Donnelly et al. (1990). Upper limits on the existence of a hard component are represented by triangles. All of the plotted data are listed in Table 2.

[7] The alert reader may note that the separate luminosities do not always sum to the corresponding luminosity shown in Fig. 1. The luminosities in Fig. 1 are taken from Donnelly et al. (1990); the original X-ray fluxes were obtained by adopting a Raymond-Smith spectrum with a temperature of 1 keV and solar abundances (see, e.g., Canizares et al. 1987; Forman et al. 1985). For sources with spectra best fitted by higher temperature models, this conversion is poor and becomes increasingly so as the temperature increases or, equivalently, as the luminosity of the hard component dominates. For NGC 507 and NGC 499, the likely explanation is the use of different apertures.

TABLE 2

SOFT AND HARD COMPONENT FLUXES

Galaxy	D^a (Mpc)	log L_B[b]	log L_X^{tot}[c]	log L_X^{soft}	log L_X^{hard}	Reference
IC 4296	72.8	11.32	41.41	41.45	41.49	1
NGC 4472.....	25.8	11.28	41.72	41.79	40.92	1
NGC 507	94.5	11.24	...	42.41	41.49	1
NGC 4649.....	25.8	11.11	41.40	41.45	40.83	1
IC 1459	43.0	11.10	40.86	40.68	41.20	1
NGC 4406.....	25.8	11.10	41.58	41.78	40.59	1
NGC 4374.....	25.8	11.02	40.79	41.15	40.63	1
NGC 4382.....	25.8	11.01	40.45	40.86	40.72	1
NGC 499	94.5	11.00	...	42.30	<41.15	1
NGC 720	39.6	10.91	41.21	41.00	40.61	1
NGC 4636.....	25.8	10.84	41.65	41.73	40.52	1
NGC 4365.....	25.8	10.82	40.29	39.82	40.49	1
NGC 5084.....	34.5	10.81	...	39.93	40.73	2
NGC 4552.....	25.7	10.77	40.61	40.64	40.29	2
NGC 1380.....	27.5	10.67	40.59	40.32	<40.39	3
NGC 4697.....	15.4	10.52	39.82	39.63	40.02	2

NOTE.—Fluxes calculated in the 0.5–4.5 keV band, listed in order of decreasing L_B.

[a] Distances from Faber et al. 1989 and Donnelly et al. 1990 (except for NGC 499 and NGC 507, distances from Kim & Fabbiano 1995, and NGC 5084, distance from recessional velocity).

[b] Luminosity in the blue band in units of $L_\odot$ and defined as $\log L_B = -0.4(M_B - 5.41)$, with M_B calculated using the distance and the B_0^T magnitude from de Vaucouleurs et al. 1991.

[c] Luminosity from Donnelly et al. 1990 based on *Einstein* fluxes and approximately representing $L_X^{soft} + L_X^{hard}$. Three galaxies are not listed in that reference.

REFERENCES.—(1) Matsumoto et al. 1997; (2) Loewenstein et al. 1997; (3) this paper.

the spectral shape then yields a more accurate estimate of the hard and soft components' luminosities. This approach is beyond the scope of this paper.

In Figure 8, the hard L_X components are plotted as diamonds (or as triangles for the upper limits of the hard components of NGC 499 and NGC 1380), and the values for the soft L_X component are plotted as squares. The luminosities of both components were calculated in the 0.5–4.5 keV band to match the *ASCA* data of Matsumoto et al. (1997). We stress again that all of the luminosities have been calculated from the same spectral model, namely, a Raymond thermal plasma that describes the soft component plus a bremsstrahlung component to represent the X-ray binary contribution.

The *ASCA* luminosity for NGC 1380 was estimated in the following manner: First, we used the software package PIMMS[8] to estimate the *ASCA* GIS count rate from the PSPC count rate. Then we adopted the best-fit PSPC spectrum, to which we added a 5 keV bremsstrahlung component with the flux in this component increased to give the 90% upper limit. We used the standard *ASCA* GIS response matrix and varied the absolute normalization of the components, while retaining the relative normalizations, until we generated the estimated count rate. We then calculated the fluxes in the defined energy bands. This approach will certainly yield a soft-band flux within 10%–15% of the correct value, because the soft, i.e., PSPC, spectrum for NGC 1380 is well defined. The hard-component flux will still be an upper limit that is good to $\sim 30\%$, which is sufficient for our purpose.

With so few data points on the plot, our intent is only to point out possible trends that must be studied in greater detail, rather than to draw a firm conclusion. Such an investigation, based on a much larger sample of *ASCA* observations, is well under way (Matsushita et al. 1997). In that spirit, however, note that the diamonds define a line near the $L_X/10^{41} \sim 0.4 L_B/10^{11}$ scaling relation. The scaling of Forman et al. (1985) does not describe the data, lying too low by about an order of magnitude. This is consistent across the extended L_B range. Either of the other scalings (Canizares et al. 1987; Fabbiano et al. 1989) can still describe the luminosity of the discrete component, particularly if the factor of 3 variation (Canizares et al. 1987) remains valid. This confirms the results presented in Matsumoto et al. (1997) for the upper end of the L_B range.

We fitted the luminosity data for the hard component using the "EM" and the Buckley-James (BJ) methods' survival statistics (see, e.g., Isobe, Feigelson, & Nelson 1986). The fit values for both methods were identical, differing only in the third decimal place. A formal fit to all of the hard-component points yields a slope (coefficient K in eq. [2]) of 1.52 ± 0.34, with a standard deviation for the regression of 0.59 (EM) or 0.65 (BJ). This fit is highly sensitive to the hard contributions of three very luminous galaxies (IC 4296, NGC 507, IC 1459), which are also the three most distant galaxies for which a hard component was detected. Two of these galaxies (IC 4296, IC 1459) are known to have active nuclei, so that the hard component may be enhanced in the 0.2–2.0 keV band. The third (NGC 507) has a steep luminosity function (Trentham 1997), which has been interpreted as a sign of current cluster formation. If we ignore all three of these galaxies, we obtain a slope of $\sim 0.42 \pm 0.07$, with a standard deviation for the regression of 0.10 (EM) or 0.11 (BJ). We note that if we believe the scaling relation implicitly and have an accurate distance for a given galaxy, the luminosity of the hard component might then be used to identify galaxies with peculiarities. For example, NGC 5084 lies at low L_B, yet the galaxy is known to be more massive (~ 4 times) than the majority of galaxies of similar type (Zeilinger, Galleta, & Madsen 1996), perhaps accounting for

[8] PIMMS is available via anonymous ftp from HEASARC at NASA GSFC.

its rather high L_X. A larger sample will be required to judge the efficacy of our conjecture for the use of the scaling relation. A larger sample is also required to assess the intrinsic scatter in the scaling relation.

A formal fit to the values for the soft component yields $L_X \sim L_B^{2.61 \pm 1.01}$ (90% error) with a dispersion of ~ 0.75. The error on the exponent is sufficiently large to encompass all of the correlations calculated by White & Davis (1997). They explored the total L_X-L_B relation from $\sim 9.5 < \log L_B < 11.0$ using *ROSAT* PSPC observations. The PSPC is sensitive largely to photons from 0.2 to 2.4 keV. White & Davis do not attempt to separate the emission, so while their results apply to contributions from the hard and soft components, the soft component dominates because of the decline in the sensitivity of the detector at energies greater than ~ 2.0 keV.[9] The dispersion we calculate is identical to the White & Davis value, so our results should then be representative of the entire sample. We also see no evidence for a break in the correlation for the soft component.

In summary, we have extended the L_X-L_B relation, decomposed separately into the discrete and hot thermal components, to $\log L_B \sim 10.5$. The scaling relation for the point-source contribution appears to be supported over approximately 1 order of magnitude in L_B. The soft ISM component exists in all of the galaxies presented here, including the faint S0 galaxy NGC 1380. NGC 1380 is supposed to show nothing but a hard component based upon its low L_B value (Fabbiano et al. 1994). Its PSPC spectrum is, however, consistent with the spectrum of a hot ISM. The spectral evidence is supported by the extended X-ray emission that is more compact than the optical profile.

Our upper limit on the emission of a hard component is not restrictive, but it dramatically illustrates our conclusion: if NGC 1380 behaved as expected (i.e., its X-ray emission resulted solely from the summed contributions of X-ray binaries), we would not have detected it. Our upper limit on the hard component of NGC 1380 must be confirmed with a more sensitive, broadband X-ray observation of NGC 1380 itself. If NGC 1380 truly lacks a hard component, then perhaps it is the first of a subset of the low-luminosity E/S0 galaxies with that property. The apparently missing hard component can, however, only be firmly demonstrated with observations of additional E/S0 galaxies of similar or fainter L_X.

The results presented here for NGC 1380 show that the total L_X of another of the very low luminosity E/S0 galaxies may be explained completely by a hot ISM component (see, e.g., Pellegrini & Fabbiano 1994 for NGC 4365 and NGC 4697; Fabbiano & Schweizer 1995 for NGC 4125 and NGC 3610). The usual assumption about the X-ray luminosity of the low-luminosity galaxies is that it is supplied solely by the summed emission of discrete sources, generally assumed to be X-ray binaries, while only the high-luminosity galaxies are expected to show evidence for a hot gaseous component. The evidence has mounted from *ROSAT* and *ASCA* data that this simple picture is misleading, and that it must be revised.

[9] I.e., at 0.75 keV, the mean temperature of the soft components from Matsumoto et al. (1997), thermal bremsstrahlung spectrum contributes $\sim 3\%$–4% of the flux in the 2.0–2.4 keV band relative to the 0.2–2.0 keV band; a 5 keV bremsstrahlung spectrum contributes about 5 times more flux in the 2.0–2.4 keV band.

We thank G. Fabbiano for comments on an early version of this paper. We thank the referee for comments that improved the paper. This work was supported under NASA contract NAG 5-4015.

REFERENCES

Buote, D., & Canizares, C. 1994, ApJ, 457, 177
Canizares, C., Fabbiano, G., & Trinchieri, G. 1987, ApJ, 312, 503
Ciotti, L., D'Ercole, A., Pellegrini, S., & Renzini, A. 1991, ApJ, 376, 380
David, L. P., Harnden, F. R., Jr., Kearns, K. E., & Zombeck, M. V. 1996, The ROSAT High Resolution Imager (HRI) Calibration Report (rev. ed.; Cambridge: US *ROSAT* Sci. Data Cent.)
Davis, D., & White, R., III. 1996, ApJ, 470, L35
———. 1997, in preparation
de Vaucouleurs, G., de Vaucouleurs, A., Corwin, H. G., Jr., Buta, R. J., Paturel, G., & Fouqué, P. 1991, Third Reference Catalogue of Bright Galaxies (New York: Springer)
Donnelly, R. H., Faber, S., & O'Connell, R. M. 1990, ApJ, 354, 52
Eskridge, P., Fabbiano, G., & Kim, D.-W. 1995, ApJS, 97, 141
Fabbiano, G. 1994, in New Horizon of X-Ray Astronomy, ed. F. Makino & T. Ohashi (Tokyo: Universal Acad.), 159
———. 1989, ARA&A, 27, 87
Fabbiano, G., Gioia, I., & Trinchieri, G. 1989, ApJ, 347, 127
Fabbiano, G., Kim, D.-W., & Trinchieri, G. 1994, ApJ, 429, 94
Fabbiano, G., & Schweizer, F. 1995, ApJ, 447, 572
Fabbiano, G., Trinchieri, G., & Canizares, C. 1986, ApJ, 310, 637
Faber, S., Wegner, G., Burstein, D., Davies, R., Dressler, A., Lynden-Bell, D., & Terlevich, R. 1989, ApJS, 69, 763
Forman, W., Jones, C., & Tucker, W. 1985, ApJ, 293, 102
Hasinger, G., Boese, G., Predehl, P., Turner, T. J., Yusaf, R., George, I., & Rohrbach, G. 1994, Legacy, 4, 40
Ikebe, Y., et al. 1996, Nature, 379, 427
Isobe, T., Feigelson, E., & Nelson, P. 1986, ApJ, 306, 490
Jahoda, K., et al. 1992, in The X-Ray Background, ed. X. Barcons & A. Fabian (Cambridge: Cambridge Univ. Press), 240
Jones, C., Stern, C., Forman, W., Breen, J., David, L., Tucker, W., & Franx, M. 1997, ApJ, 482, 143
Kim, D.-W., & Fabbiano, G. 1995, ApJ, 441, 182
Kim, D.-W., Fabbiano, G., Matsumoto, H., Koyama, K., & Trinchieri, G. 1996, ApJ, 468, 175
Kim, D.-W., Fabbiano, G., & Trinchieri, G. 1992, ApJ, 393, 134
Loewenstein, M., Mushotzky, R. F., Tamura, T., Ikebe, Y., Makishima, K., Matsushita, K., Awaki, H., & Serlemitsos, P. J. 1994, ApJ, 436, L75
Loewenstein, M., et al. 1997, in preparation
Matsumoto, H., Koyama, K., Awaki, H., Tsuru, T., Loewenstein, M., & Matsushita, K. 1997, ApJ, 482, 133
Matsushita, K., et al. 1994, ApJ, 436, L41
———. 1997, in preparation
Pellegrini, S. 1994, A&A, 292, 395
Pellegrini, S., & Fabbiano, G. 1994, ApJ, 429, 105
Pfeffermann, E., et al. 1987, Proc. SPIE, 733, 519
Roberts, M., Hogg, D., Bregman, J., Forman, W., & Jones, C. 1991, ApJS, 75, 751
Sarazin, C. 1990, in The Interstellar Medium in Galaxies, ed. H. A. Thronson, Jr., & J. M. Shull (Dordrecht: Kluwer), 201
Schlegel, E. M., & Petre, R. 1993, ApJ, 412, L29
Snowden, S. 1995, Cookbook for Analysis Procedures for *ROSAT* XRT/PSPC Observations of Extended Objects and the Diffuse Background (rev. ed.; Greenbelt, MD: GSFC)
Snowden, S., McCammon, D., Burrows, D., & Mendenhall, J. 1994, ApJ, 424, 714
Stark, A. A., Gammie, C. F., Wilson, R. W., Bally, J., Linke, R. A., Heiles, C., & Hurwitz, M. 1992, ApJS, 79, 77
Trentham, N. 1997, MNRAS, 286, 133
Trinchieri, G., Kim, D.-W., Fabbiano, G., & Canizares, C. 1994, ApJ, 428, 555
van den Bergh, S., & Tammann, G. 1991, ARA&A, 29, 363
White, R., III, & Davis, D. 1997, in ASP Conf. Ser. 115, Galactic and Cluster Cooling Flows, ed. N. Soker (San Francisco: ASP), 217
White, R., III, & Sarazin, C. 1991, ApJ, 367, 476
Zeilinger, W., Galleta, G., & Madsen, C. 1990, MNRAS, 246, 324